

Supplementary Information

Cell type-specific genetic and optogenetic tools reveal novel hippocampal CA2 circuits

Keigo Kohara^{1,*}, Michele Pignatelli^{1,*}, Alexander J. Rivest¹, Hae-Yoon Jung¹, Takashi Kitamura¹, Junghyup Suh¹, Dominic Frank¹, Koichiro Kajikawa¹, Nathan Mise^{2,†}, Yuichi Obata², Ian R. Wickersham³ and Susumu Tonegawa^{1,4}

¹RIKEN-MIT Center for Neural Circuit Genetics at the Picower Institute for Learning and Memory, Department of Biology and Department of Brain and Cognitive Sciences, Massachusetts Institute of Technology, Cambridge, Massachusetts 02139, USA

²RIKEN BioResource Center, 3-1-1 Koyadai, Tsukuba, Ibaraki 305-0074, Japan

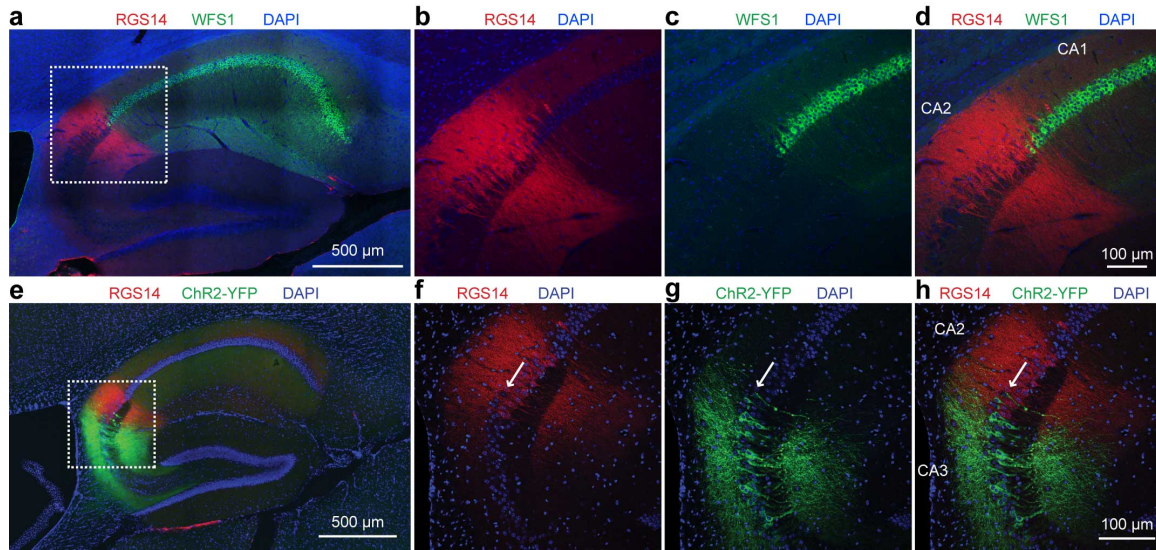
³Media Lab, Massachusetts Institute of Technology, Cambridge, Massachusetts 02139, USA

⁴Howard Hughes Medical Institute, Massachusetts Institute of Technology, Cambridge, MA 02139, USA

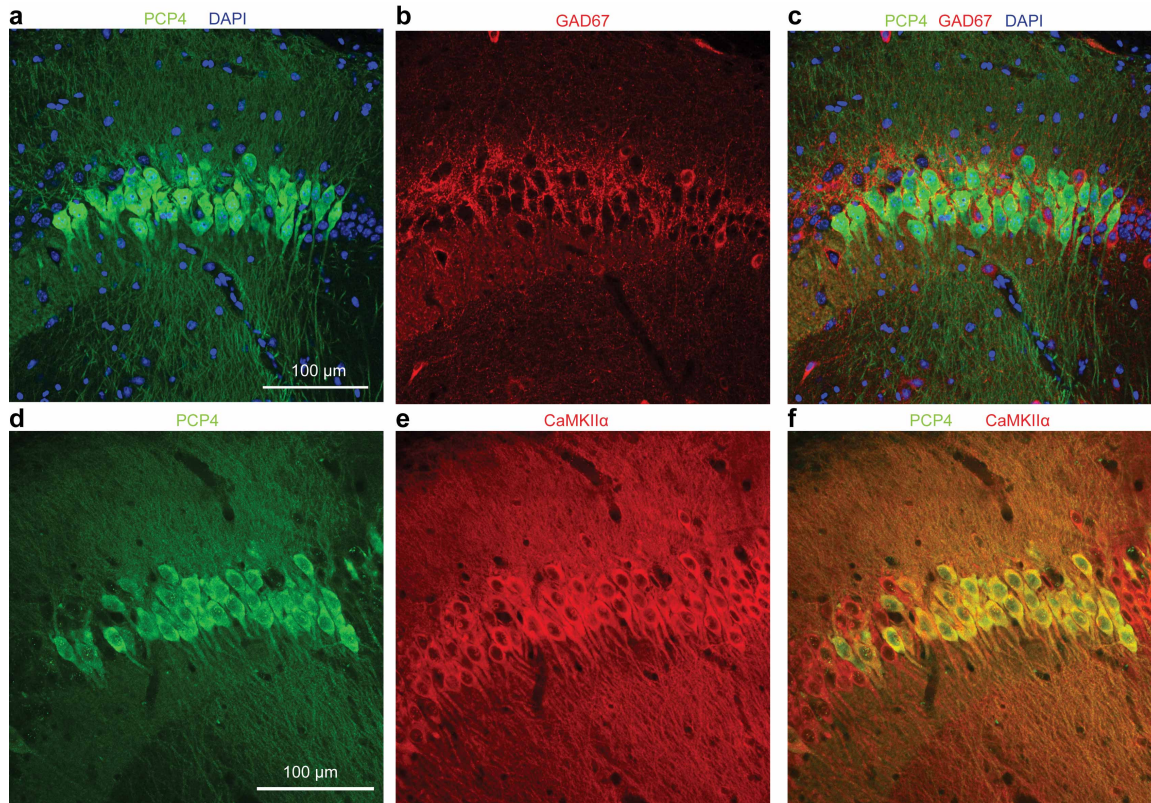
[†]present address: Department of Environmental Preventive Medicine, Jichi Medical University, Tochigi 329-0498, Japan

*These authors contributed equally to this work

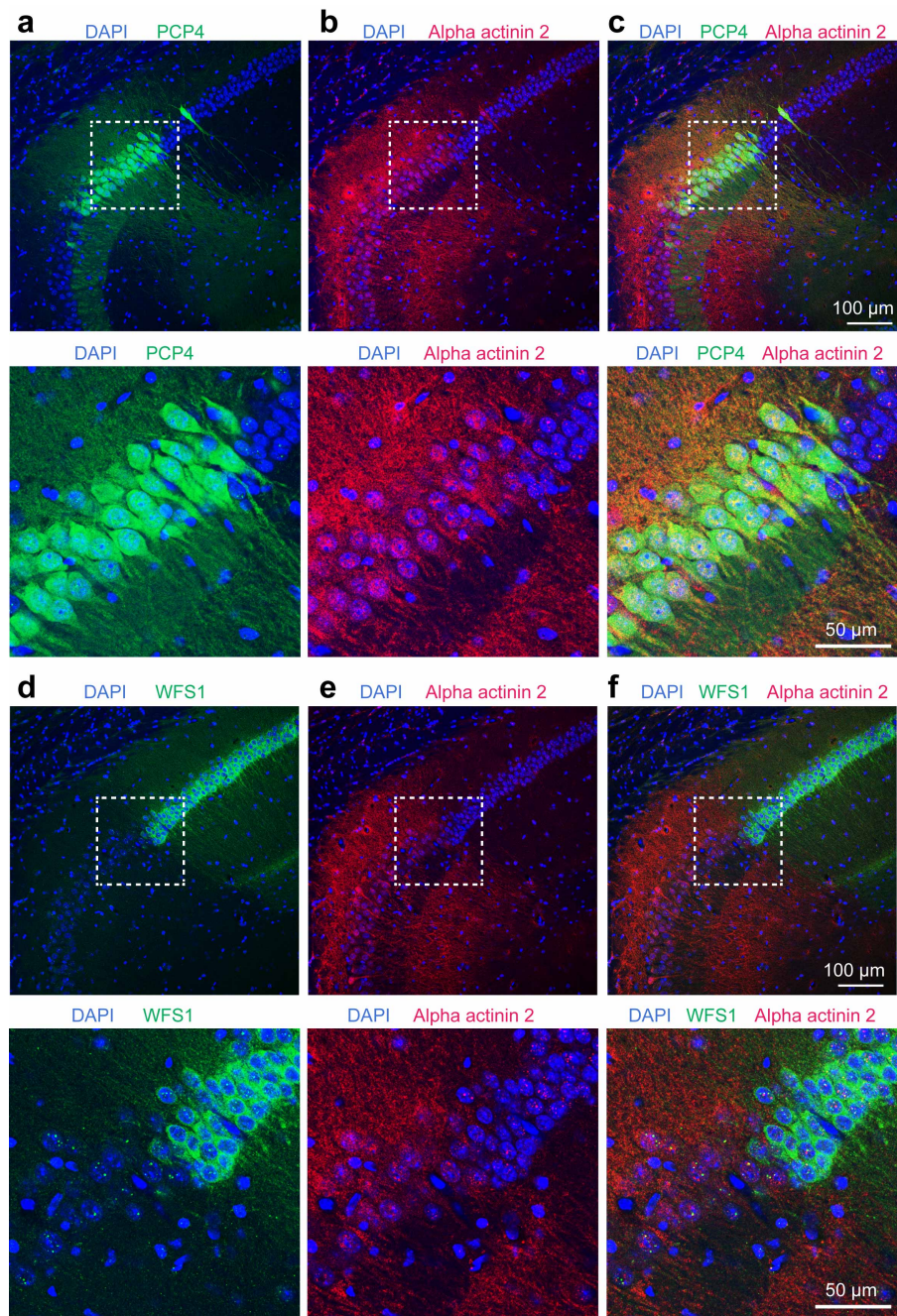
1. Supplementary Figures and Legends



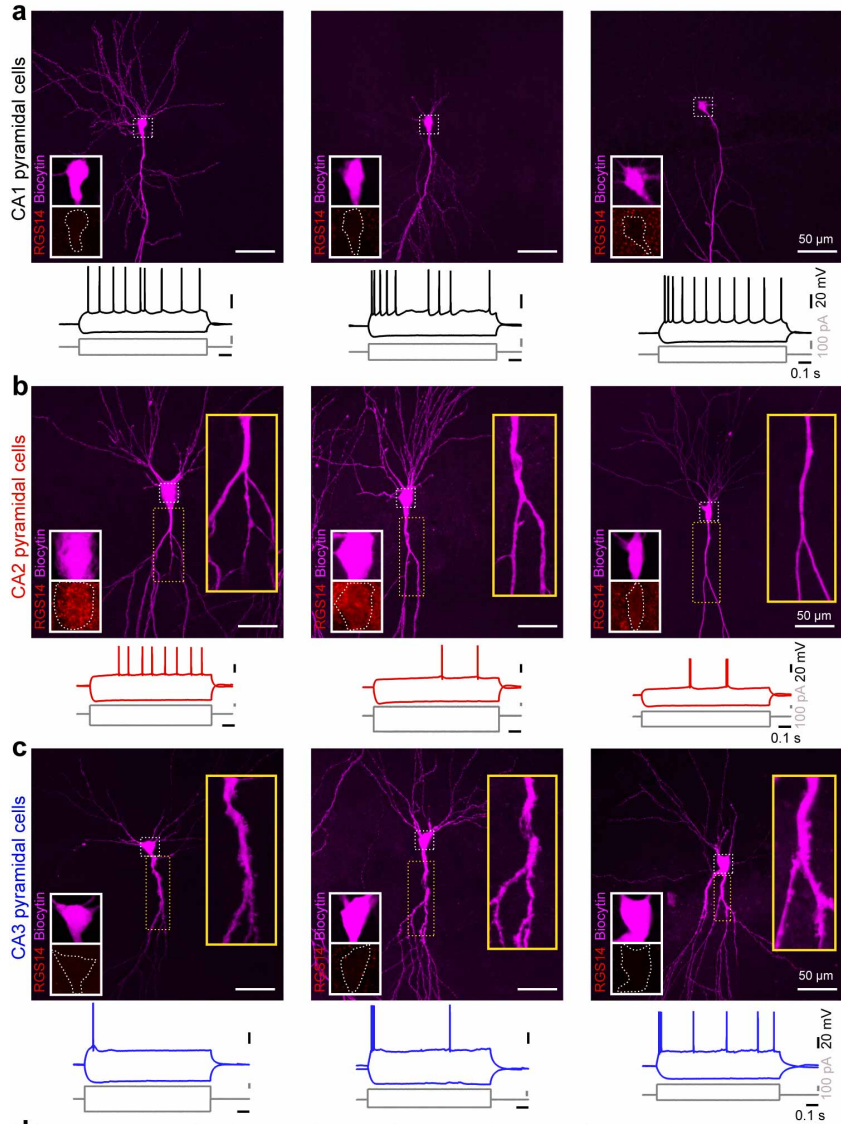
Supplementary Figure 1: Segregated expression of CA1, CA2, and CA3 gene markers. **a**, Representative image displaying a segregated expression of CA2 gene marker (RGS14, red) and CA1 gene marker (WFS1, green) in a wild type mouse. **b-d**, Confocal images from the dotted line-box in **(a)** showing RGS14 expression **(b)**, WFS1 expression **(c)**, and overlay between RGS14 and WFS1 **(d)**. Note the precise segregation between CA1 and CA2. **e**, CA2 gene marker, RGS14 (red), is not expressed in CA3 as shown by the segregation with ChR2-YFP, specifically expressed in a CA3 Cre transgenic mouse. **f-h**, Confocal images from the dotted line-box in **(e)** showing RGS14 expression **(f)**, ChR2-YFP expression **(g)** and overlay between RGS14 and ChR2-YFP **(h)**. Note the intermingled expression of the CA3 transgenic marker in RGS14-negative cells in CA2 (arrows).



Supplementary Figure 2: CA2 gene markers are specifically expressed in the excitatory and not in inhibitory neurons in the pyramidal cell layer. Single confocal stacks (**a-i**). **a**, Overlay of DAPI and PCP4 staining, a CA2 marker. **b**, The same CA2 region stained for GAD67, a marker of inhibitory cells. **c**, Lack of colocalization of PCP4 and GAD67 markers. **d**, PCP4 staining. **e**, The same CA2 region stained for CaMKII α , a marker of excitatory cells. **f**, Colocalization (yellow) of PCP4 and CaMKII α markers.

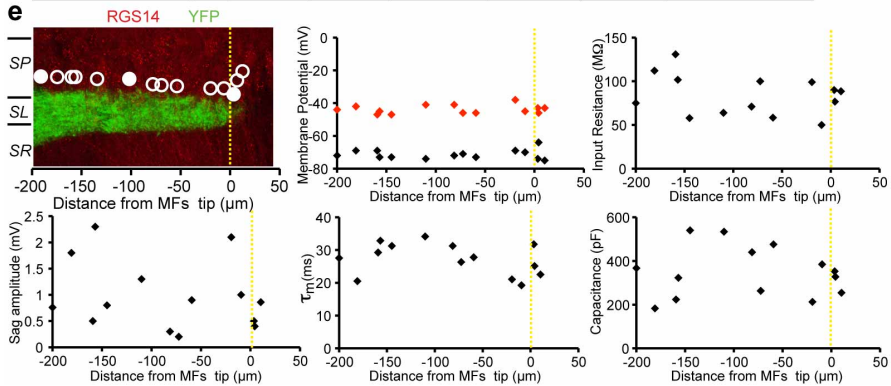


Supplementary Figure 3: CA2 cells PCP4-positive express α -actinin2. **a**, PCP4 staining. **b**, The same field stained for α -actinin2. **c**, All PCP4-positive cells express α -actinin2 (60 cells out of 60 from n=3 mice, sampled from the entire CA2 region). In the region following the mossy fiber ending, most of α -actinin2-positive cells express PCP4 (~90%, 56 out of 62 from n=3 mice) and the few PCP4-negative cells (~10%, 6 out of 62) may include interneurons because α -actinin2 is also expressed in interneurons (Ratzliff & Soltesz, Neuroscience, 2001). Bottom: magnification from the dotted line-box. **a**, WFS1 staining. **b**, The same field stained for α -actinin2. **c**, WFS1-positive cells do not express α -actinin2. Bottom: magnification from the dotted line-box.

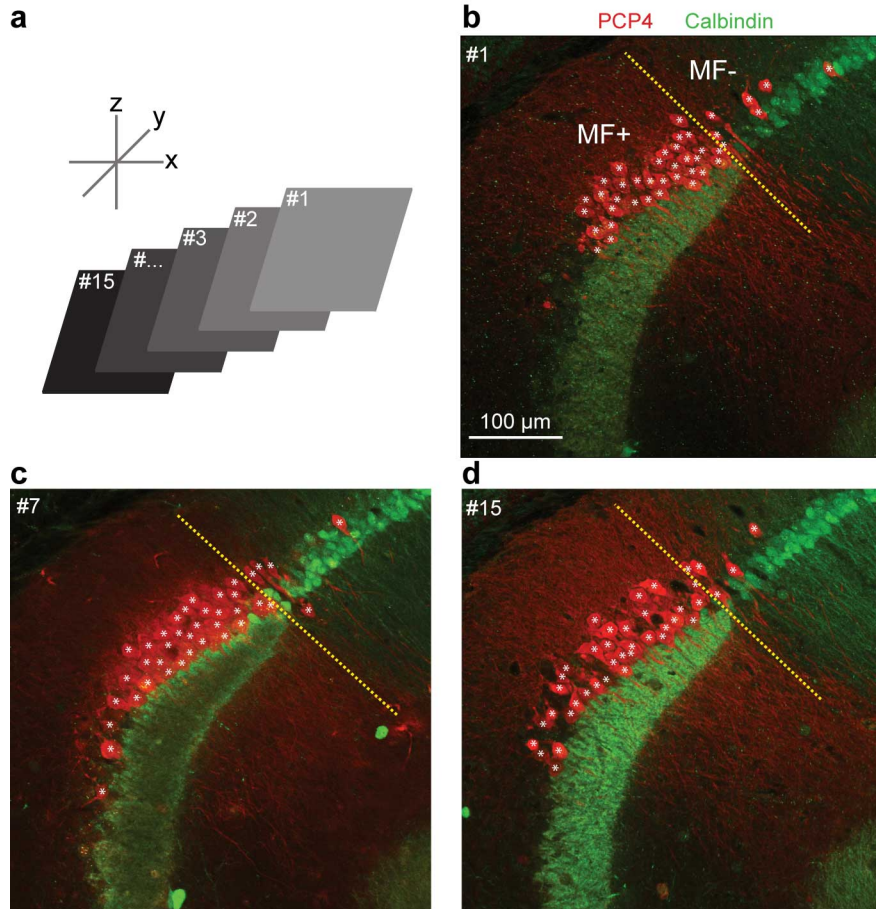


d

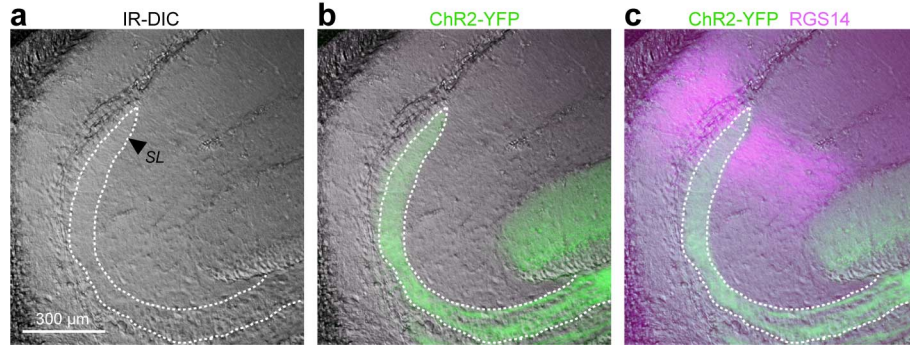
Cell Type	n	V _m mV	Ri MΩ	AP _{thr} mV	Sag mV	τ _m ms	Capacitance pF
CA1	9	-70±09	128±7.4	-49±0.7	2±0.2	16±1	129±11
CA2	14	-70±1	78±6.2	-44±0.7	0.98±0.18	27±1	349±31
CA3	11	-72±1.5	155±18	-43±1.4	0.8±0.14	24±4	152±10
CA2-CA1 ttest P		0.3	0.0003	0.00002	0.0007	0.00001	0.000005
CA2-CA3 ttest P		0.008	0.003	0.7	0.4	0.4	0.00001
CA1-CA3 ttest P		0.002	0.2	0.001	0.0001	0.07	0.14



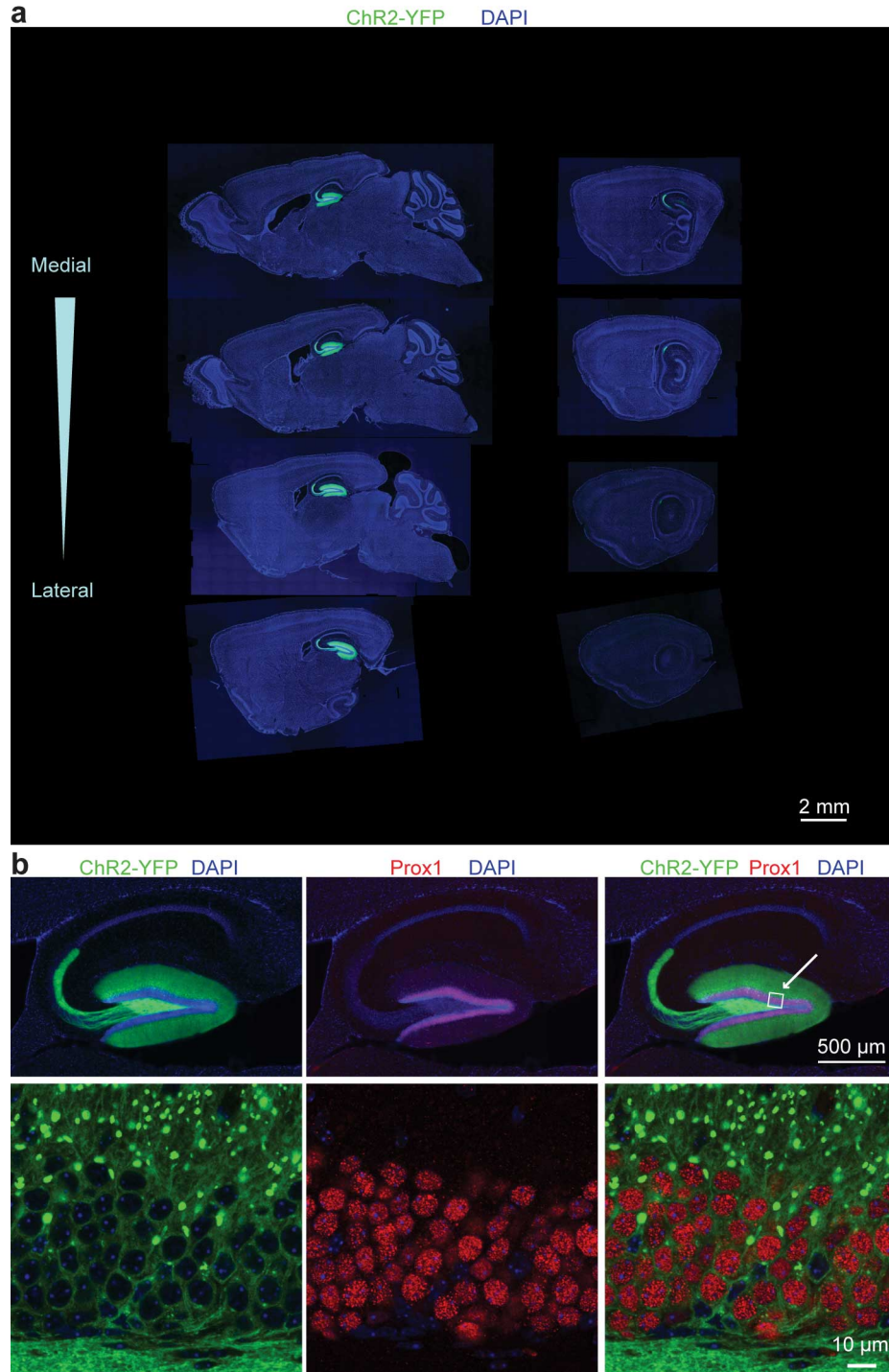
Supplementary Figure 4: Morphology and intrinsic electrophysiological properties of CA1, CA2 and CA3 pyramidal cells. **a**, Confocal images (Z-projection, top) and intrinsic electrophysiological properties (bottom) of three CA1 pyramidal cells stained with biocytin. Inset from the white dotted line-box: RGS14 staining shows no overlay. **b**, Confocal images (Z-projection, top) and intrinsic electrophysiological properties (bottom) of three CA2 pyramidal cells stained with biocytin. Inset from the white dotted line-box: RGS14 staining of CA2 pyramidal cells. Yellow inset from the yellow dotted line-box: magnification of the apical dendrite. Note the lack of complex dendritic spines. **c**, Confocal images (Z-projection, top) and intrinsic electrophysiological properties (bottom) of three CA3 pyramidal cells stained with biocytin. Inset from the white dotted line-box: RGS14 staining shows no overlay. Yellow inset from the yellow dotted line-boxes: magnification of the apical dendrites. Note the complex spines on the apical dendrites. **d**, Summary table of the intrinsic electrophysiological properties of CA1, CA2 and CA3 pyramidal cells (V_m resting membrane potential, R_i input resistance, AP_{thr} action potential threshold, τ_m membrane time constant). Significant differences, tested with a two tailed unpaired t-test, in bold. **e**, Schematic illustrating the positions (white circles) of the n=14 CA2 pyramidal cells analyzed in (**d**) relative to the end (yellow dotted line) of mossy fibers (MFs). Filled white circles represent proximal, middle and distal CA2 pyramidal cells respectively, as illustrated from left to right in (**b**). Green: mossy fibers. Red: RGS14-positive CA2 region. SP: stratum pyramidale, SL: stratum lucidum, SR: stratum radiatum. On the side: scatter plots showing the relationship between distance from the MFs tip and intrinsic properties. Membrane potential (black dots: resting membrane potential; red dots: action potential threshold), Input resistance, Sag amplitude, Membrane time constant, Capacitance.



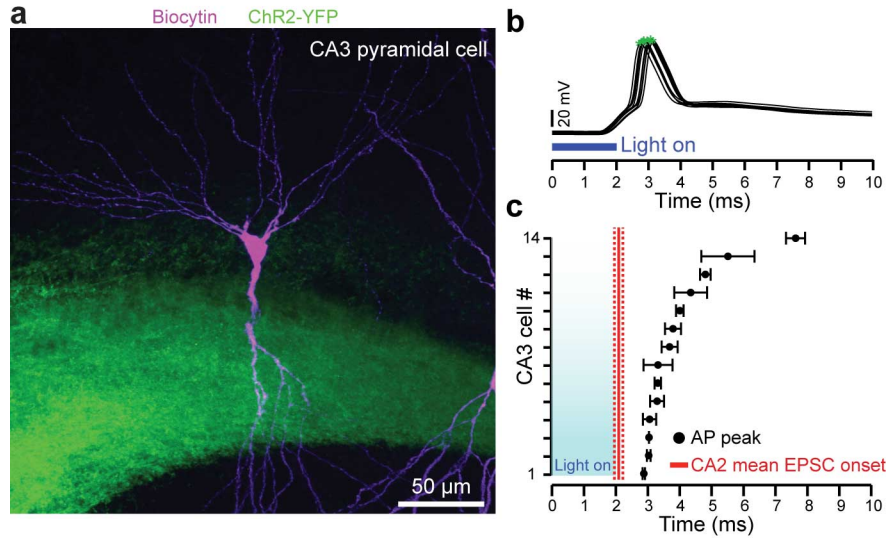
Supplementary Figure 5: Estimation of CA2 cell number overlapping with mossy fibers (MF+) and not overlapping with mossy fibers (MF-). **a**, A sequential series of images acquired by confocal microscopy (n=15 images per sample every 1.5 μm). **b-d**, Mossy fibers were stained for calbindin (green) and CA2 pyramidal cells for PCP4 (red). All the PCP4-positive cells (red) were identified on a single focal plane (asterisks, white) and grouped into two classes depending on whether they overlapped with mossy fibers (MF+ class) or they did not (MF- class). The dotted yellow line, parallel to the apical dendrites, indicates the distal end of the mossy fibers. Note the presence of calbindin positive cells in the CA1 pyramidal layer.



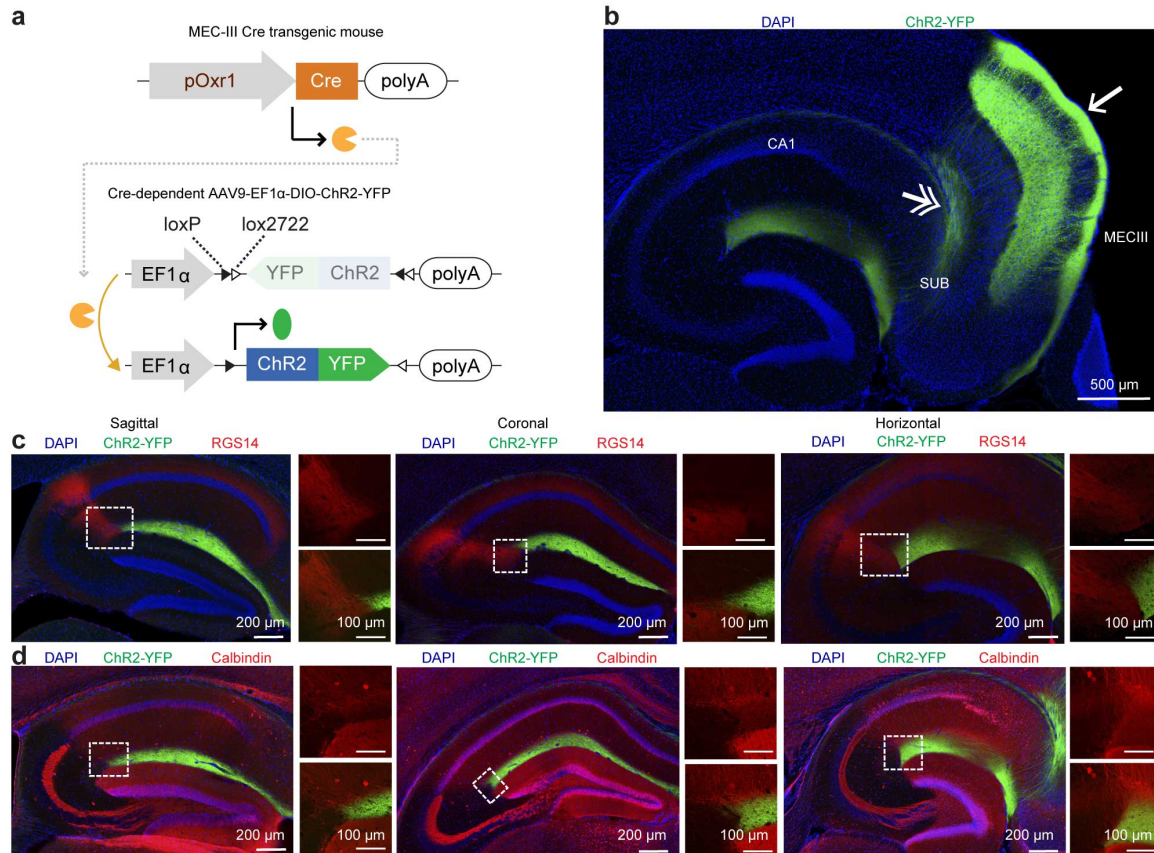
Supplementary Figure 6: The CA2 component of mossy fibers run exclusively in the stratum lucidum. **a**, DIC image of the CA2 region. Arrowhead: stratum lucidum (SL) outlined by the dotted line. **b**, The same image displaying ChR2-YFP-positive mossy fibers in green. **c**, Same image as (**b**), displaying in addition the RGS14-positive CA2 region (pink).



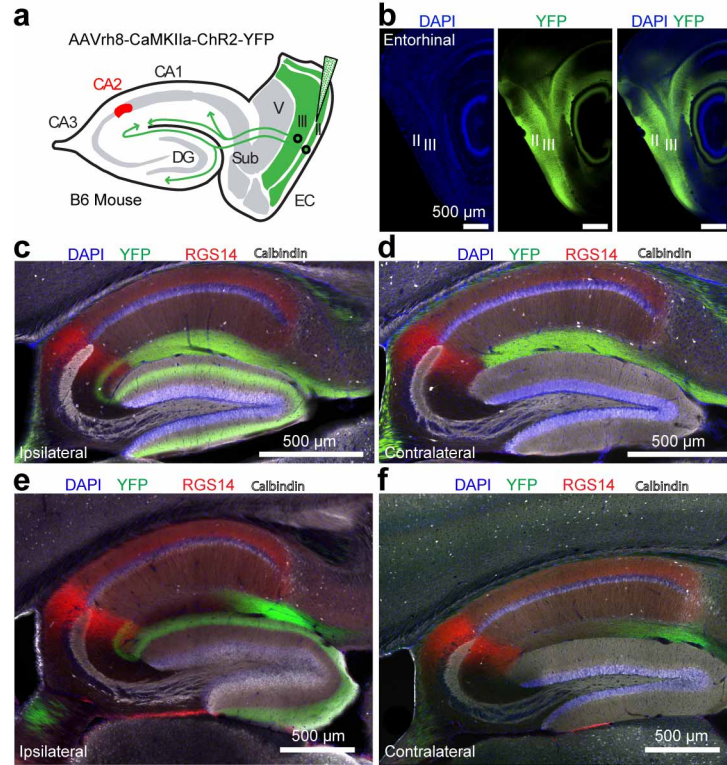
Supplementary Figure 7: Dentate gyrus expression of ChR2-YFP in Dock10 Cre mice is specific to dentate granule cells. **a**, ChR2-YFP expression (green) is selective for dentate gyrus and mossy fibers throughout the medial-lateral axis. **b**, Almost all ChR2-YFP-positive cells express Prox1, a dentate granule cell specific marker mainly selective to adult granule cells. Lower panels: confocal stacks from the dotted line-box (arrow).



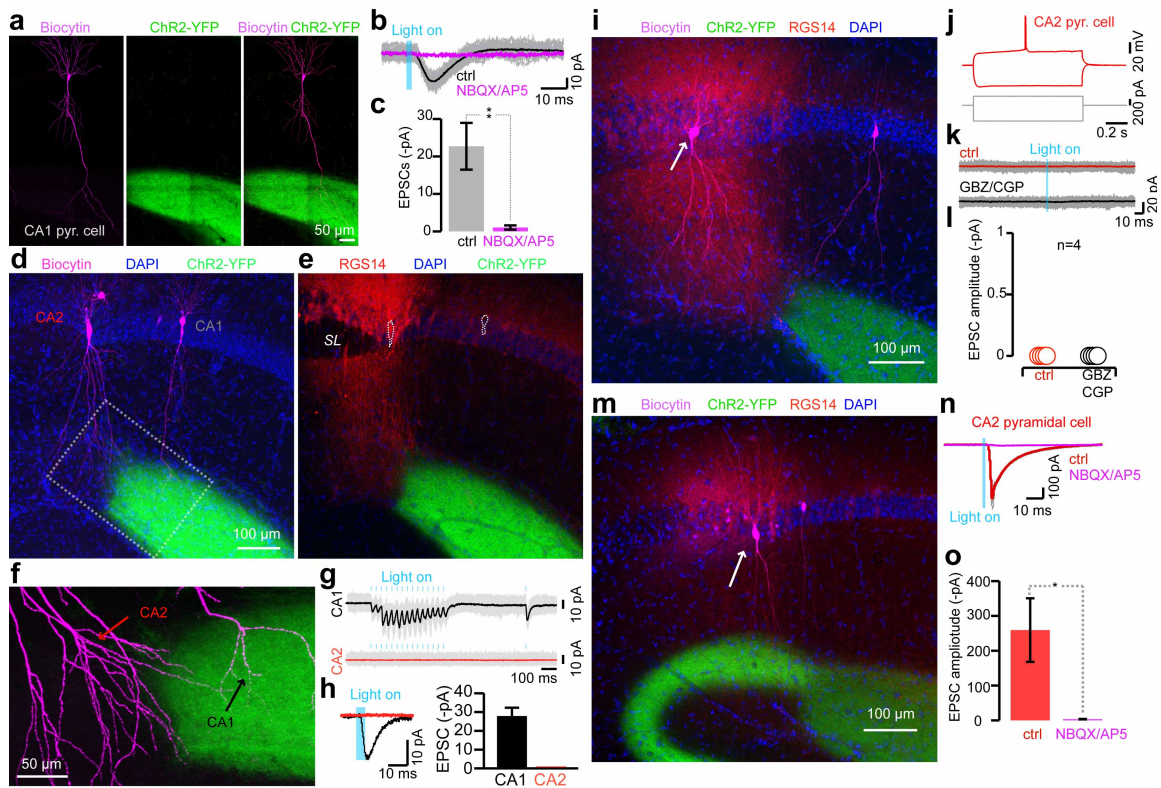
Supplementary Figure 8: CA3 pyramidal cell action potential (AP) peak time in response to optogenetic activation of mossy fibers. **a**, Representative image of a recorded CA3 pyramidal cell stained by biocytin (violet). Note the ChR2-YFP-positive mossy fibers in green. **b**, Optogenetic activation of mossy fibers elicited spiking activity in a CA3 pyramidal cell (same from **a**) recorded in current mode. Note the AP peak times (green asterisks). **c**, AP peak times from $n=14$ CA3 pyramidal cells responding to optogenetic activation of mossy fibers. The red line indicates the mean EPSC onset (\pm SEM) of CA2 pyramidal cells in response to mossy fiber activation. The onset of the EPSCs recorded in CA2 pyramidal cells always precedes the AP peak of CA3 pyramidal cells. Error bars represent standard error of the mean.



Supplementary Figure 9: Medial entorhinal cortex layer III (MECIII) pyramidal neuron projections do not overlap with RGS14-positive CA2 region in all the anatomical planes. **a**, Diagram depicting MECIII-specific *pOxr1*-Cre transgenic mouse injected with Cre-dependent AAV9-EF1 α -DIO-ChR2-YFP. Cre-recombinase switches on the expression of ChR2-YFP in MECIII cells. **b**, Confocal image of a horizontal slice depicting projection pattern resulting from **(a)**. Subiculum (SUB), CA1, and MECIII are labeled. Note MECIII dendrites in MECI (single-headed arrow) and fibers crossing from MECIII into the hippocampus (double-headed arrow). **c**, MECIII projections (ChR2-YFP, green) into the hippocampus costained for RGS14 (red) and DAPI (blue): sagittal (left), coronal (middle), and horizontal (right) sections. Dotted line-boxes indicate the regions of inset images to the immediate right. Inset images show RGS14 staining on top, and RGS14 staining overlaid with the MECIII-specific YFP signal on bottom. Note the lack of overlap between the YFP (green) and the RGS14 (red) signal. **d**, Sections cut on the same planes as in **(c)** stained for calbindin, a CA1 pyramidal cell marker, and data organized as in **(c)**. Insets from dotted line-boxes: note the overlap and co-termination of the YFP (green) signal and calbindin (red) staining.

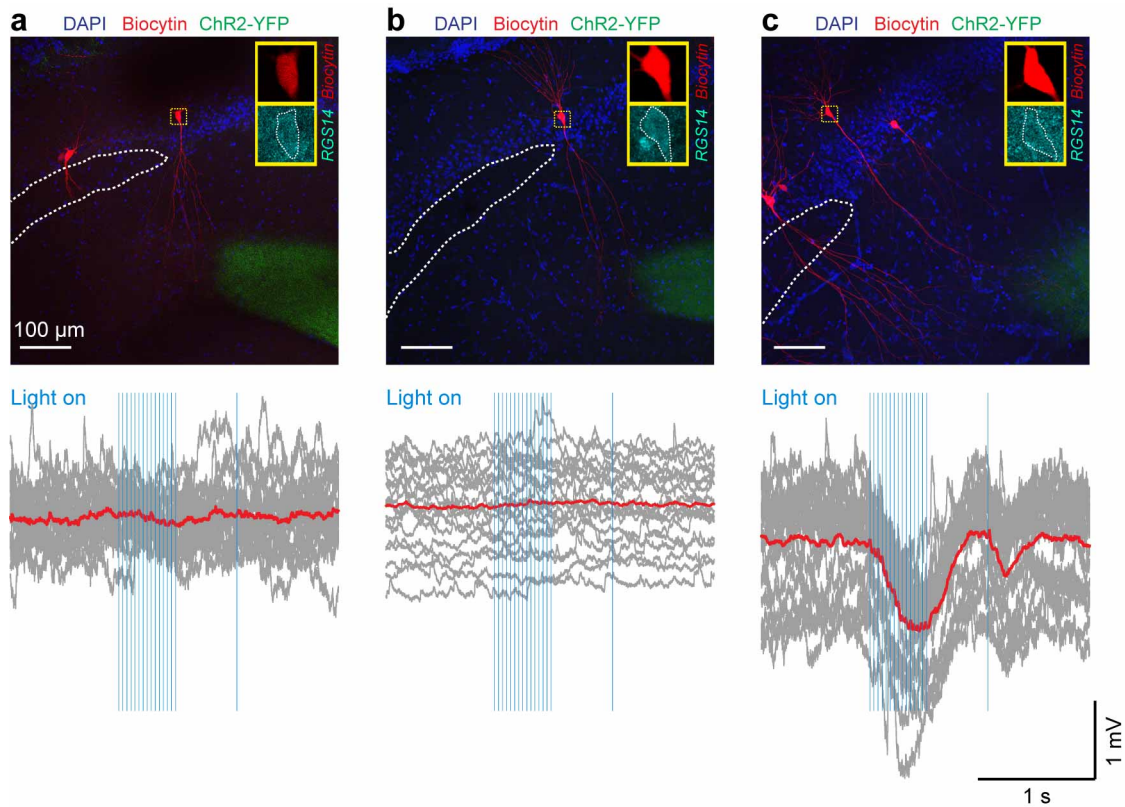


Supplementary Figure 10: Anatomical segregation between two cortico-hippocampal circuits in wild-type mice: ECIII→CA1 and ECII→DG/CA2/CA3. **a**, Experimental design depicting the injection of a non-Cre-dependent AAVrh8-CaMKIIa-ChR2-YFP into the superficial medial entorhinal area of wild type mouse. **b**, Confocal image of a sagittal slice depicting YFP expression near the injection site in the MEC. **c**, Ipsilateral sagittal hippocampus section of infected mouse depicted in (**b**). Tissue stained for calbindin (white), RGS14 (red) and with DAPI (blue) and ChR2-YFP (green) expression. Both MECIII (terminating in CA1-SLM) and MECII fibers (terminating in DG, CA3 and CA2) can be seen. MEC-specific infection is confirmed by distribution of YFP in the middle one-third of the dendrites of the DG. **d**, Contralateral sagittal hippocampal section of the same mouse in (**c**) with same staining as (**c**). On the contralateral side, no MECII fibers can be detected, and MECIII fibers form a sharp boundary with the CA2-specific RGS14 staining. **e**, Ipsilateral sagittal hippocampus section of wild type mouse infected with AAVrh8-CaMKIIa-ChR2-YFP in the superficial lateral entorhinal cortex (LEC). Tissue stained for calbindin (white), RGS14 (red) and DAPI (blue) and ChR2-YFP (green) expression. Both LECIII (terminating in SLM of CA1) and LECII fibers (terminating in DG, CA3 and CA2) can be seen. LEC infection is confirmed by expression of YFP in the outer one-third of the dendrites of the DG. Note: the distribution of the YFP-positive LECIII fibers in CA1-SLM does not reach the proximal end of CA1. Note that YFP-labeled LECII fibers overlap with RGS14-positive CA2 region. **f**, Contralateral sagittal hippocampal section of mouse depicted in (**e**) with same staining as (**e**). On the contralateral side, no LECII fibers can be seen, and LECIII fibers only reach the distal regions of CA1, far away from the RGS14 signal.

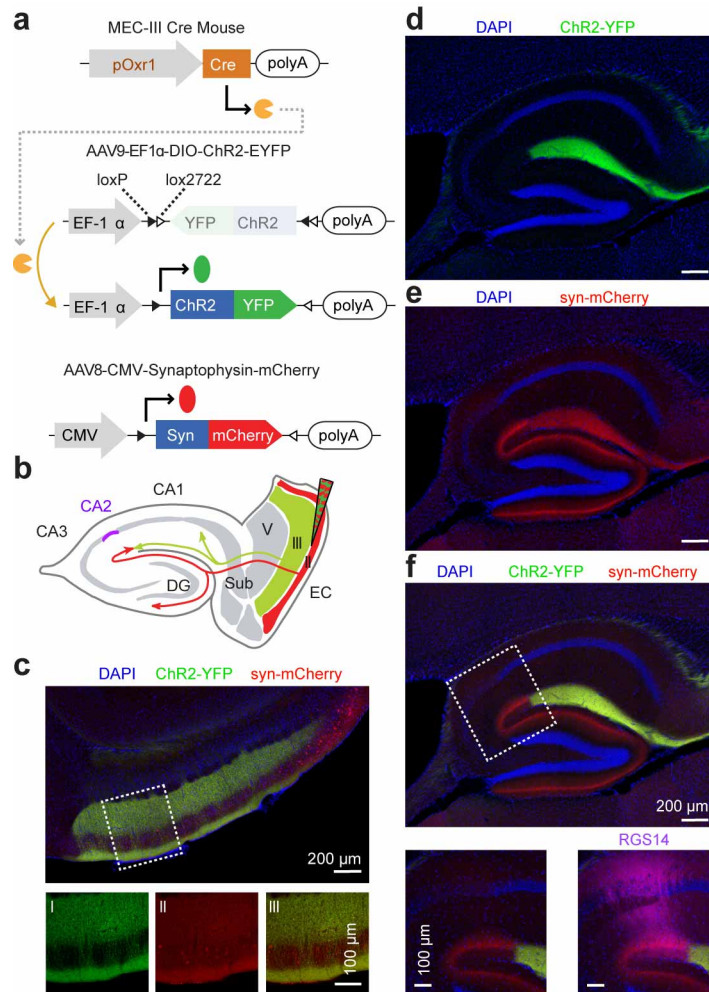


Supplementary Figure 11: Optogenetic stimulation of MECIII and MECII fibers. **a-c**, Glutamatergic synaptic transmission recorded in CA1 pyramidal cells in response to optogenetic stimulation of MECIII fibers. **(a)** Zeta-projected confocal image of a recorded CA1 pyramidal cell stained with biocytin (violet). Note ChR2-YFP-positive MECIII fibers (green) running in the stratum lacunosum-moleculare (SLM). **(b)** Optogenetic stimulation of MECIII fibers (green) elicited an excitatory synaptic response in the same CA1 pyramidal cell displayed in **(a)**. The response was sensitive to bath application of NBQX (10 μ M) and AP5 (100 μ M). Average of 30 traces in black (control: ctrl) and NBQX/AP5 in violet **(b)**. **(c)** Average EPSCs amplitude in control and under bath application of NBQX and AP5 ($n=7$, $**KS<0.005$). **d-l**, MECIII fibers do not establish functional synaptic connections with CA2 pyramidal cells. **(d)** Zeta-projected confocal image of a biocytin-filled (violet) CA1 and CA2 pyramidal cells recorded in the same slice. **(e)** Confocal image showing the same sample stained for the RGS14. SL: stratum lucidum. Only the CA2 pyramidal cell expresses RGS14. Note the location of the CA2 cell away from stratum lucidum. **(f)** ChR2-YFP-positive MECIII fibers (green) overlap with the CA1 apical dendrite, but very little with the CA2 dendrites, enlarged from the dotted-line box in **(d)**. **(g)** Patch-clamp recordings of the same pair of cells as in **(d)**. Optogenetic stimulation of MECIII fibers (green) with an augmented stimulation protocol, a 30 Hz train of 15 light pulses elicited EPSCs in CA1 but not in CA2 pyramidal cells. **(h)** Recording and mean response of CA1 (black, $n=18$) and CA2 (red, $n=10$) cells (same as Fig. 6d) to a 5 ms light pulse activating MECIII fibers ChR2-positive. Only CA1 pyramidal cells responded. **(i)** Zeta-projected confocal image of a recorded CA1 and CA2 (arrow) pyramidal cells, both stained with biocytin (violet). Note ChR2-YFP-positive MECIII fibers (green) running in the SLM and the RGS14 staining (red) defining the CA2 region. **(j)** Electrophysiological recording of the same CA2 pyramidal cell in **(i)** in response to current step injections. **(k)** Optogenetic stimulation of MECIII fibers (green) did not elicit an excitatory synaptic response in the same CA2 pyramidal cell, even in presence of blockers of GABAergic transmission (GBZ 10 μ M and CGP 2 μ M). **(l)** The same result was observed in $n=4$ CA2 pyramidal cells. **m**, Zeta-projected confocal image of a recorded CA1 and CA2 (arrow) pyramidal cell, both stained with biocytin (violet). Note ChR2-YFP-positive MECII fibers (green) and the RGS14 staining (red) defining the CA2 region. **n**, Optogenetic stimulation of MECII fibers (green) elicited an excitatory synaptic response in the same CA2 pyramidal cell displayed in **(m)**. The response was sensitive to bath application of NBQX (10 μ M) and AP5 (100

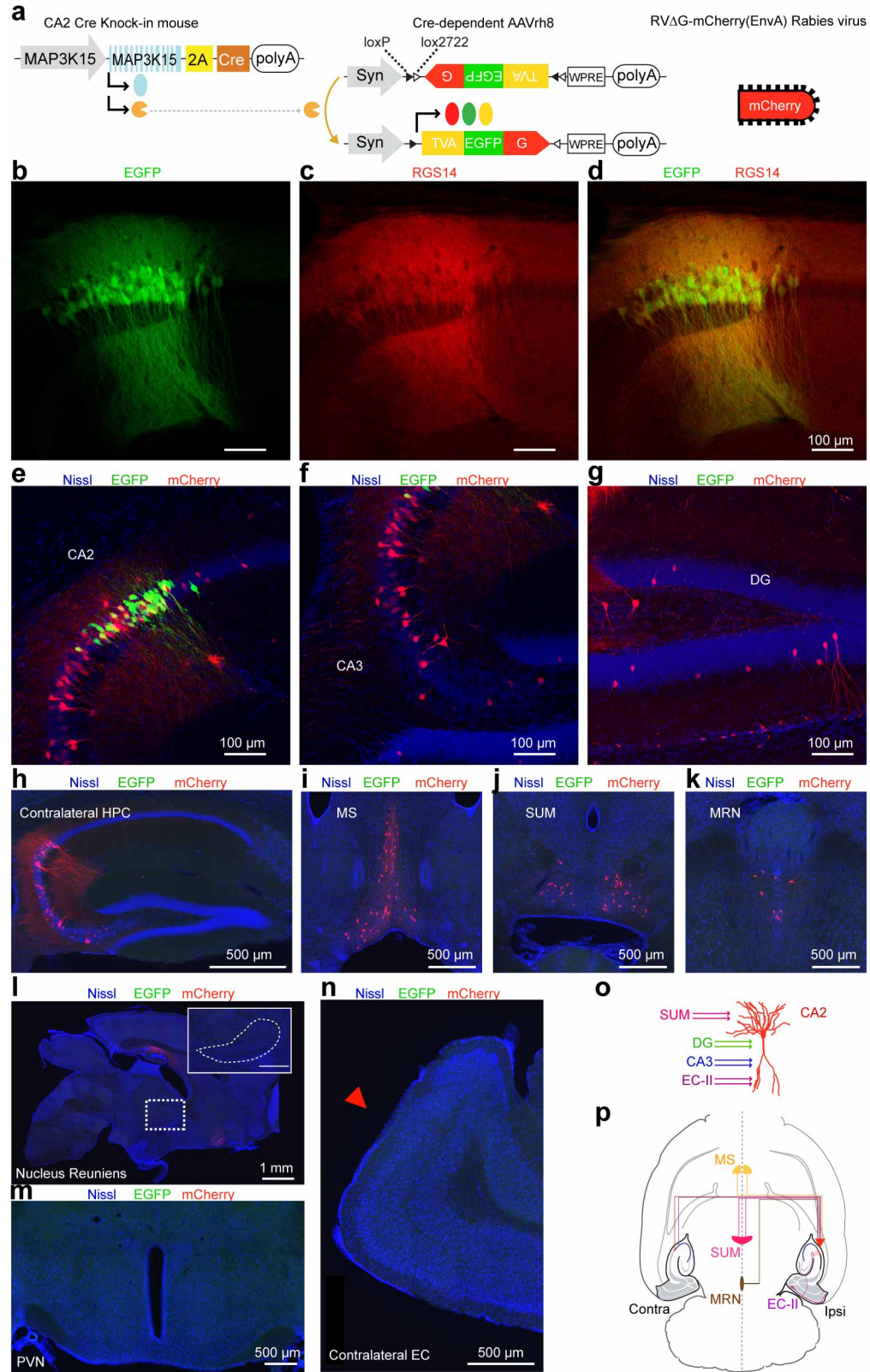
μM). Average of 30 traces in red and NBQX/AP5 in violet. **o**, Average EPSCs amplitude in control and under bath application of NBQX and AP5 ($n=4$, $*KS<0.05$). Data are represented as $\text{mean}\pm\text{SEM}$.



Supplementary Figure 12: Lack of excitatory synaptic transmission in distal CA2 pyramidal cells in response to optogenetic stimulation of MECIII. **a-c**, Z-projected confocal images of biocytin filled distal CA2 pyramidal cells (red). Note the ChR2-YFP-positive MECIII fibers in green. Dotted line: stratum lucidum. Inset from the dotted line-boxes in yellow: magnified single confocal stacks showing biocytin filled CA2 pyramidal cells RGS14-positive. Bottom: electrophysiological recordings in current mode (averages in red) of the same CA2 cells in response to optogenetic stimulation of MECIII fibers (30 Hz train followed 500 ms later by a single recovery light pulse). Note in (c) the presence of a strong polysynaptic inhibition.

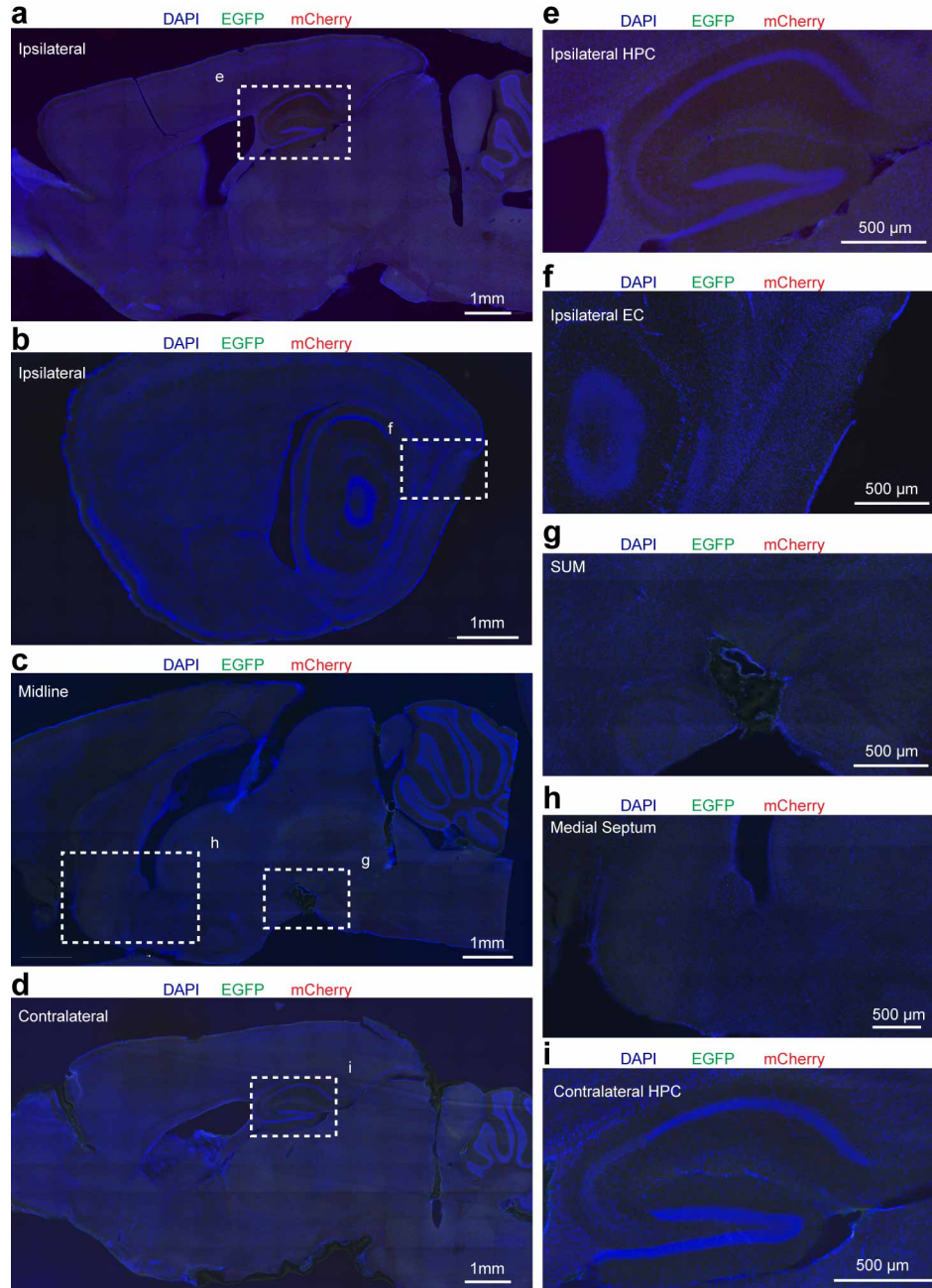


Supplementary Figure 13: Mutually exclusive cortico-hippocampal circuits: ECIII→CA1 and ECII→DG/CA2/CA3. **a**, Diagram depicting *pOxr1*-Cre mouse injected with two viruses: Cre-dependent AAV9-EF1 α -DIO-ChR2-YFP and non-Cre-dependent AAV8-CMV-Synaptophysin-mCherry. **b**, Schematic of double virus injection from **(a)** and expression patterns in the entorhinal cortex (EC) as well as the projection patterns into the hippocampus. **c**, Sagittal EC section of injection area showing mCherry and YFP expression. Insets from the dotted-line box: mCherry labeling in MECII and in MECIII (II, III) and YFP only labeling MECIII and not MECII or any other cell type (I, III). Fibers in MECI are pyramidal MECIII dendrites. **d**, Sagittal section showing MECIII fiber projection (YFP, green) into the SLM region of the CA1 area. **e**, Same section showing MECIII and MECII synaptophysin-labeled terminals (red). **f**, Overlay of **(d)** and **(e)**. Note the yellow signal in CA1-SLM indicating coexpression of MECIII-specific YFP and mCherry signals, as well as the lack of YFP in the U-turn indicating MECII exclusive projection. Bottom: enlarged confocal images from the dotted line-box showing RGS14 staining (purple) of the CA2 region. Note the overlap between RGS14-positive CA2 dendrites and putative MECII fibers, but not with MECIII fibers.

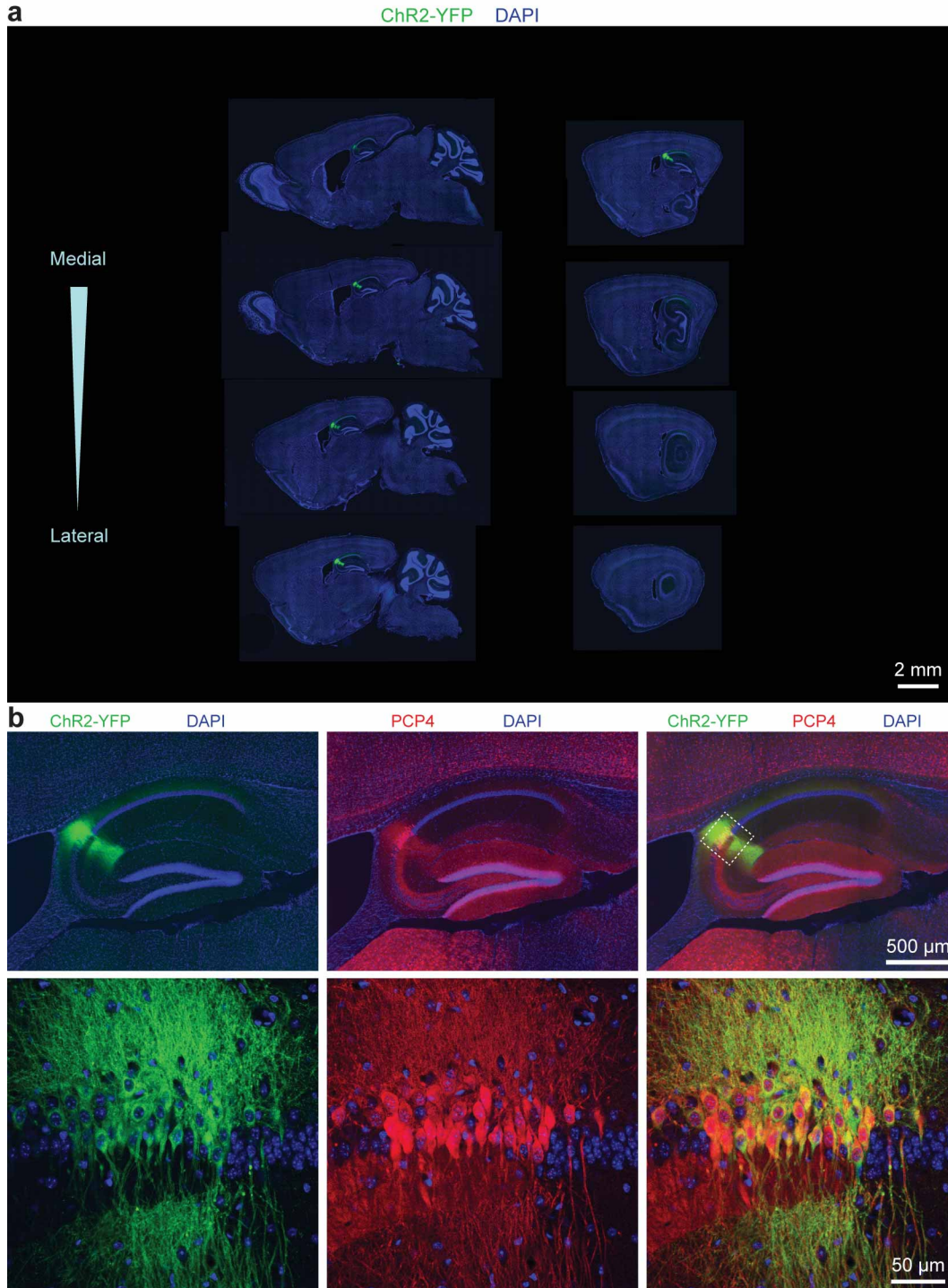


Supplementary Figure 14: Whole-brain mapping of direct inputs to hippocampal CA2 pyramidal cells using the rabies virus-based monosynaptic tracing. **a**, Diagram depicting CA2-specific *MAP3K15*-Cre

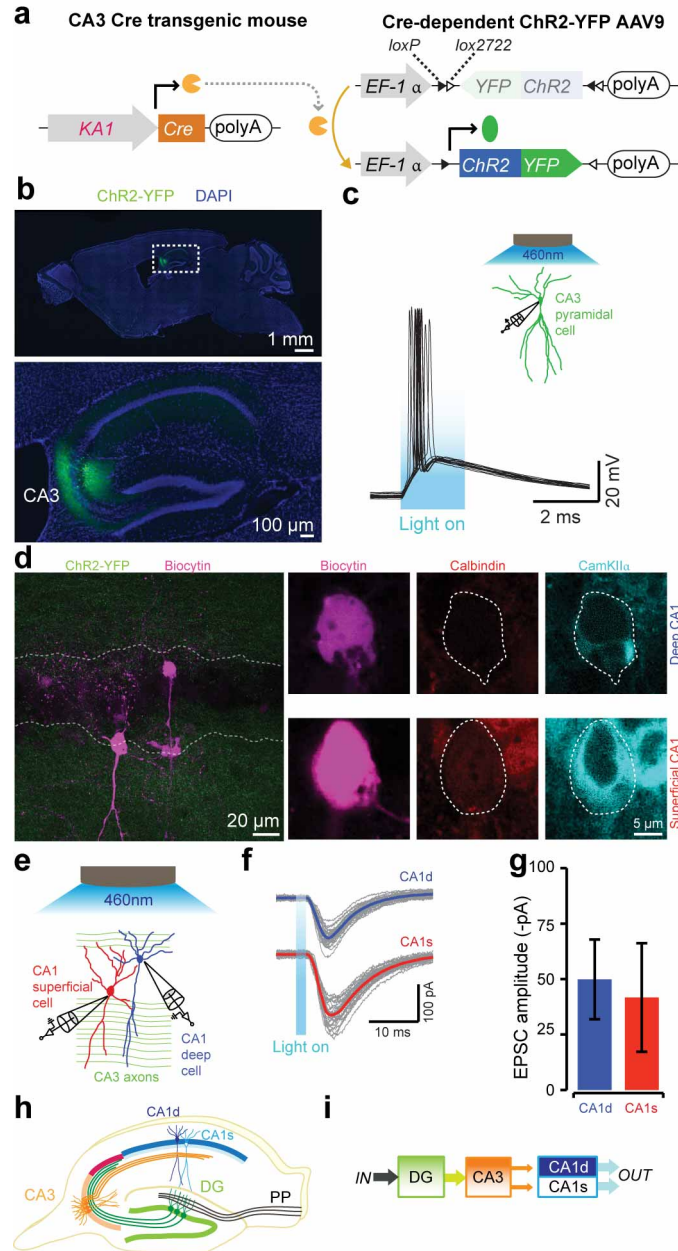
mouse injected with two viruses: Cre-dependent rabies helper AAV, followed 7 days later by mCherry-expressing rabies virus (RV). **b-d**, Colocalization of RGS14 with EGFP from a *MAP3K15*-Cre mouse infected with AAVrh8-FLEX-TVA-EGFP-RG19. (b) EGFP signal (green) 14 days after infection. (c) RGS14 staining (red) on same section as (b). (d) Overlap of (b) and (c). 95.1% of EGFP-positive cells were also RGS14-positive (369 of 388 EGFP-positive neurons were RGS14-positive in 8 sections from 4 animals). **e-n**, Sections stained with Nissl (blue) and imaged for mCherry-positive cells and EGFP-positive cells. **e-g**, Sagittal section from the ipsilateral hippocampus shown in Fig. 7c displaying mCherry-only positive cells in CA2 (e), CA3 (f), and DG (g). **h-k**, Neurons presynaptic to CA2, as labeled by mCherry-only signal, in the CA2 and CA3 of the contralateral hippocampus (h), medial septum (MS) (i), supramammillary nucleus (SUM) (j), and median raphe nucleus (MRN) (k) from the mouse shown in Fig. 7c. **l-n**, We observed no mCherry-positive cells in the nucleus reuniens, in the paraventricular nucleus of the hypothalamus, or in the contralateral entorhinal cortex. (l) Parasagittal midline section showing lack of mCherry signal in the nucleus reuniens. Inset from dotted line-box shows the outlined nucleus reuniens (scale bar is 500 μ m). (m) Coronal section showing lack of mCherry signal in the paraventricular nucleus of the hypothalamus. (n) Horizontal section of contralateral dorsal entorhinal cortex (red arrowhead). No mCherry signal was detected in any of the contralateral EC sections analyzed. **o**, Presynaptic wiring diagram for CA2 pyramidal cells. **p**, Presynaptic wiring diagram for CA2 pyramidal cells showing contralateral hippocampal, ipsilateral entorhinal and subcortical afferents. MS: medial septum, SUM: supramammillary nucleus, MRN: median raphe nucleus.



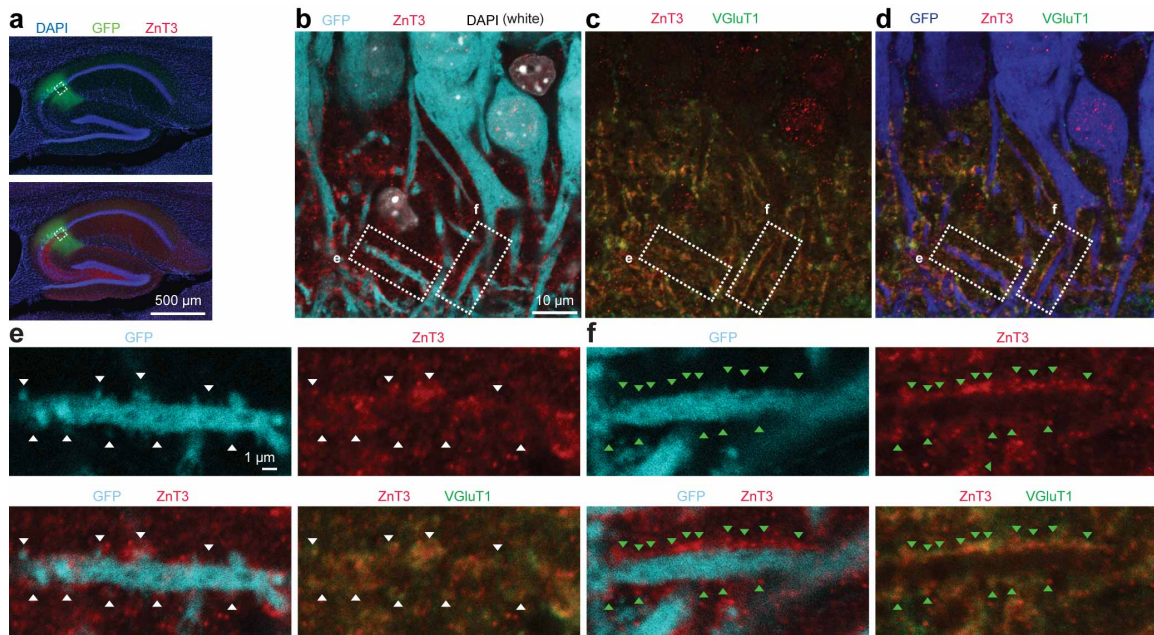
Supplementary Figure 15: Infection of AAVrh8-FLEX-TVA-EGFP-RG19 and RVΔG-mCherry(EnvA) into wild type mice revealed no mCherry signal outside of the injection area. **a-d**, Whole brain sagittal sections centered on: **(a)** ipsilateral section showing hippocampus from the same position as Fig. 7c, **(b)** ipsilateral entorhinal cortex, **(c)** midline subcortical structures, and **(d)** contralateral side containing the hippocampus. **e-i**, Inset magnification from the dotted line-boxes in **(a-d)**. **(e)** Ipsilateral hippocampus, **(f)** ipsilateral entorhinal cortex, **(g)** supramammillary nucleus (SUM), **(h)** medial septum, and **(i)** contralateral hippocampus. No EGFP or mCherry signal was detected in any of these regions.



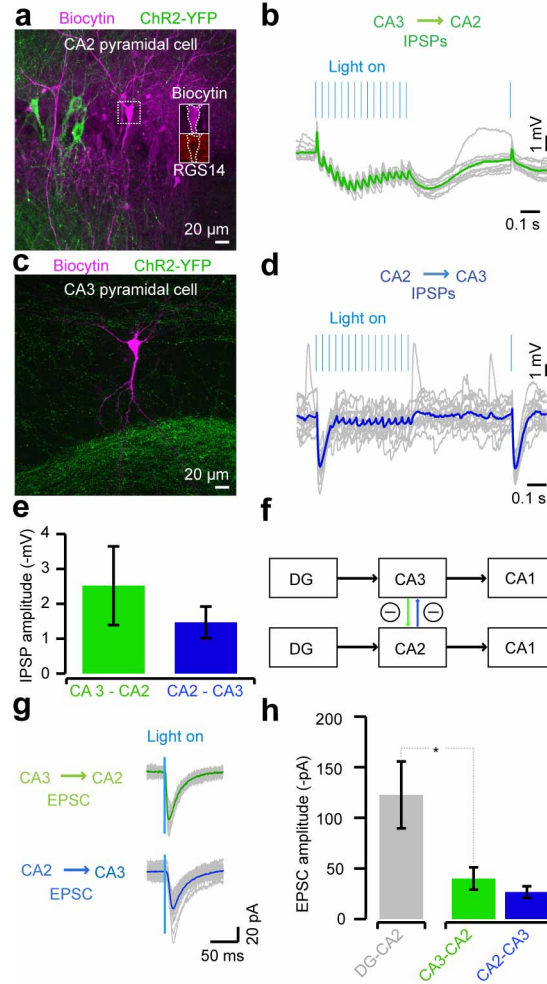
Supplementary Figure 16: CA2 pyramidal cells-specific expression of ChR2-YFP in MAP3K15 Cre mice. **a**, ChR2-YFP expression (green) is selective for the CA2 pyramidal cells throughout the medial-lateral axis. **b**, ChR2-YFP positive cells express PCP4, a CA2 gene marker. Note the axonal projections into CA1 stratum oriens. Lower panels: confocal images from the dotted line-box showing coexpression of ChR2-YFP and PCP4.



Supplementary Figure 17: CA3 pyramidal cells innervate the CA1 sublayers with equal strength. **a**, CA3-specific transgenic Cre mice were injected with Cre-dependent AAV9-EF1 α -ChR2-YFP. Cre-recombinase switches on the expression of ChR2-YFP in CA3. **b**, CA3-specific expression of ChR2-YFP (top) and enlarged images from the dotted line-box (bottom). **c**, Optogenetic stimulation of a ChR2-YFP-positive CA3 pyramidal cell. **d**, Representative z-projected image of a pair of recorded CA1 pyramidal cells located in different sublayers (dotted line: pyramidal cell layer). Upper side-panels: deep CA1 cell CaMKII α -positive and calbindin-negative. Lower side-panels: superficial CA1 cell CaMKII α -positive and calbindin-negative. **e**, Optogenetic stimulation of CA3 fibers combined with patch-clamp recordings of CA1 superficial (red) and deep pyramidal cells (blue) sampled in the same hippocampal slice. **f-g** Optogenetic stimulation of CA3 fibers elicited an equal response in the CA1 sublayers ($n=7$, $P=0.62$). **h-i**, Classic trisynaptic circuit mediated by CA3. Data are represented as mean \pm SEM.



Supplementary Figure 18: Confocal microscopy analysis of synaptic connections between mossy fibers and CA2 pyramidal cells. **a**, Representative image showing GFP labeled CA2 pyramidal cells (green) in CA2-specific Cre knock-in mouse (top). Bottom: same sections stained for ZnT3 (red), a presynaptic marker of mossy fibers. **b**, GFP-positive CA2 pyramidal cell dendrites (light blue) in the stratum lucidum are surrounded by ZnT3-positive clusters (red). **c**, ZnT3 colocalizes with VGluT1. **d**, GFP-positive CA2 pyramidal cell dendrites (blue) are surrounded by ZnT3-VGluT1 double-positive clusters. Dotted line-boxes in panel **b**, **c** and **d**, are respectively magnified in panel **e** and **f**. **e**, Magnification from the dotted line-box (**e**) showing a GFP-positive CA2 dendrite in the stratum lucidum. The dendrite has simple spines (white arrowheads) surrounded by ZnT3-VGluT1 double-positive clusters. **f**, Magnification from the dotted line-box (**f**) showing a GFP-positive CA2 dendrite in the stratum lucidum. The dendritic shaft (green arrowheads) is surrounded by ZnT3-VGluT1 double-positive clusters.



Supplementary Figure 19: Reciprocal inhibition between the two trisynaptic circuits at the CA3→CA2 and CA2→CA3 junctions. **a**, Biocytin stained CA2 pyramidal cell. Inset: the same cell stained for RGS14. Note the ChR2-YFP-positive CA3 fibers from CA3-specific transgenic Cre mice injected with Cre-dependent AAV9-EF1 α -ChR2-YFP. **b**, Electrophysiological response (green) of the same cell to optogenetic stimulation of CA3 fibers. Note the inhibitory response. Cell recorded in current clamp configuration. Inhibition was observed in 6 out of 8 connections. **c**, Biocytin stained CA3 pyramidal cell. Note the ChR2-YFP-positive CA2 fibers from CA2-specific knock-in Cre mice injected with Cre-dependent AAV9-EF1 α -ChR2-YFP. **d**, Electrophysiological response (blue) of the same cell to optogenetic stimulation of CA2 fibers. Note the inhibitory response. Cell recorded in current clamp configuration. Inhibition was observed in 6 out of 10 connections. **e**, Average IPSP amplitude for CA3-CA2 connection (amplitude measured on the first pulse, n=6, green) and for CA2-CA3 connection (amplitude measured on the first pulse, n=6, blue). Two-tailed unpaired t-test $P=0.42$. **f**, Schematic summarizing the reciprocal inhibition between the two trisynaptic circuits occurring at the CA3→CA2 (green) and CA2→CA3 connections (blue). **g**, Representative voltage clamp recordings of EPSCs displayed by CA3-CA2 (green) and CA2-CA3 (blue) connections in response to optogenetic stimulation of CA3 or CA2 fibers respectively. Holding voltage -70 mV. **h**, Average EPSC amplitude for dentate to CA2 (DG-CA2, n=23, gray), CA3 to CA2 (CA3-CA2, n=10, green) and CA2 to CA3 (CA2-CA3, n=13, blue) connections. DG-CA2 connections display larger amplitude than CA3-CA2 connections (two-tailed unpaired t-test $*P<0.05$). CA3-CA2 and CA2-CA3 connections display similar strengths (two-tailed unpaired t-test $P=0.3$). Data are represented as mean \pm SEM.